Solitary-wave conduction in *p*-type Ge under time-dependent voltage bias

Michael J. Bergmann* and Stephen W. Teitsworth†
Department of Physics and the Center for Nonlinear and Complex Systems, Duke University, Durham, North Carolina 27708-0305

Luis L. Bonilla‡
Universidad Carlos III de Madrid, Escuela Politécnica Superior, 28 913 Leganés, Madrid, Spain

Inma Rodríguez Cantalapiedra§
Departamento Física Aplicada Universidad Politécnica de Cataluña, c/Gregorio Marañón 44-50, 08 028 Barcelona, Spain

(Received 30 June 1995; revised manuscript 27 September 1995)

We present the results of numerical simulations of a drift-diffusion model—including electric-field-dependent generation-recombination processes—for closely compensated *p*-type Ge at low temperature and under dc+ac and dc+noise voltage biases, with an Ohmic boundary condition. We observe frequency locking and quasiperiodicity under dc+ac bias, but do not find chaotic behavior for a uniform impurity profile. Noise-induced intermittent switching near the onset of solitary-wave conduction is compared to experimentally observed intermittency, type-III intermittency, and on-off intermittency. For a linearly increasing acceptor concentration, we find that the size of the solitary waves diminishes as they advance across the sample.

I. INTRODUCTION

Many semiconductor systems driven far from thermodynamic equilibrium display nonlinear electrical conduction. For sufficiently large current densities or electric fields, nonlinear conduction arises from various microscopic processes, such as impact ionization [Ge (Refs. 1 and 2) and GaAs (Ref. 3)], enhanced impurity trapping [*n*-type Ge (Ref. 4)], momentum-space transfer [GaAs (Refs. 5 and 6)], real-space transfer in semiconductor heterostructures,[7,8] and sequential resonant tunneling in superlattices.[9,10] The onset of nonlinear conduction is associated frequently with qualitative changes in the macroscopic behavior of the system, which may be described as a nonequilibrium phase transition.[11] Recently, there has been much interest in the spatiotemporal dynamics of such nonequilibrium systems.[12–14] Ultrapure extrinsic cooled bulk *p*-type Ge is ideally suited to the study of spatiotemporal behavior in driven dissipative systems. The signal to noise ratio is large (≈ 80 dB), and the dynamical length scale (mm) and time scale (ms) of the spatiotemporal structures make accurate data collection convenient and rapid.[15]

The onset of nonlinear conduction processes can be seen typically in the stationary, spatially homogeneous current density $j_{\rm sh}(\mathscr{E})$, where $\mathscr{E}$ is the electric field. For positive differential resistance, fluctuations in the system decay and the stationary, spatially homogeneous state is stable; however, for negative differential resistance (NDR) the stationary, spatially homogeneous state may become unstable to spatiotemporal structures.[16] The NDR in our model of the *p*-type Ge system arises from negative differential carrier concentration due to the generation and recombination dynamics of holes from shallow acceptor impurities. Instabilities arising from negative differential carrier concentration have also been reported for GaAs,[4] InSb,[17] and Si.[18] We find that the NDR in our model arises from a negative differential impact-ionization rate and is only present in closely compensated samples. The NDR produces a "N" shaped $j_{\rm sh}(\mathscr{E})$ curve (NNDR),[19] as shown in Fig. 1.

We focus on biases that cause the spatially averaged electric field (voltage divided by sample length) to be above the value for impurity breakdown. For such biases, NDR,[20] large current oscillations,[20,21] and spatiotemporal structures[15,22–25] have been observed in experiments. We use a set of rate equations within the drift-diffusion approximation—including electric-field-dependent impact-ionization and recombination rates and an electric-field-dependent drift velocity[26,27] —to model the spatiotemporal dynamics of the system. Bonilla has previously employed asymptotic analysis to make predictions for the spatial dependency of the steady-state electric field,[28] the onset voltage to small-amplitude periodic current oscillations,[28–30] and the stability of moving high-field domains[31] [which is closely related to the stability analysis for Gunn domains in GaAs (Ref. 32)]. In earlier numerical simulations under dc voltage bias, we observed

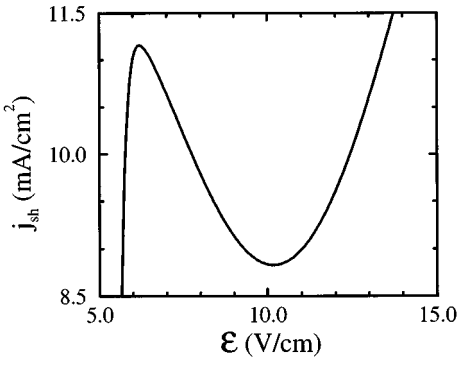

FIG. 1. The homogeneous stationary current density $j_{\rm sh}(\mathscr{E})$ for $\alpha = 1.21$, illustrating the NDR in our model.

electric-field solitary waves that travel periodically across the sample,[19,29,33] which have wave speed and wave size in close agreement with the experiments of Kahn, Mar, and Westervelt.[15] In this paper, we examine the effect of adding an ac signal to the dc bias, the relationship between external noise in the dc bias and intermittency, and the spatiotemporal dynamics that result from having a linearly increasing acceptor concentration. The addition of noise to the bias and the spatial variation of the acceptor concentration result in behavior that was absent in our previous simulations,[19,29,33] but is found in the experimental system,[15,24] in particular, intermittency and shrinking space-charge waves.

The paper is organized as follows. Section II contains a brief review of the model equations. In Sec. III, the sample is biased with a dc+ac voltage, and we observe quasiperiodicity and frequency locking, but find no evidence of chaos above the critical line. In Sec. IV, we add a small white-noise term to the dc voltage bias, as an approximation to external noise, and find intermittent switching between two periodic states. We find in Sec. V that a small linear variation in the impurity profile across the sample produces solitary waves that shrink as they propagate. In the conclusion we discuss the discrepancies that remain between our model and experiment, principally the differing statistics of the intermittent switching and the absence of chaos. Appendix A contains the functional forms of electric-field-dependent impact-ionization and recombination coefficients and the electric-field-dependent drift velocity. Appendix B is a description of the numerical algorithm used in our simulations.

II. MODEL SYSTEM

We use a standard drift-diffusion description of the hole current, electric-field-dependent generation and recombination of free holes, and Poisson's law to model carrier transport.[26,34,35] We simplify the description by neglecting the displacement current and the diffusive component of the hole current.[34] The problem may be reformulated then as a ''reduced equation'' in terms of a single spatially dependent field variable, the electric field, and the spatially homogeneous current density.[28,34] The reduced equation is

$$V(E)^{-1}\frac{dJ}{d\tau}=\frac{\partial^2 E}{\partial x\,\partial\tau}+c_1(E,J)\frac{\partial E}{\partial\tau}+c_2(E,J)\frac{\partial E}{\partial x}+c_3(E,J), \tag{1a}$$

$$c_1(E,J)=\frac{J}{V(E)^2}V'(E), \tag{1b}$$

$$c_2(E,J)=\frac{J[K(E)+R(E)]}{V(E)}, \tag{1c}$$

$$c_3(E,J)=[J_{\rm sh}(E)-J]\frac{c_2(E,J)}{V(E)}, \tag{1d}$$

$$J_{\rm sh}(E)=\left[\frac{\alpha K(E)}{K(E)+R(E)}-1\right]V(E), \tag{1e}$$

where $V'(E)=dV/dE$. Here $E(x,\tau)$ is the dimensionless electric field and $J(\tau)$ is the dimensionless current density. The functions $K(E)$, $R(E)$, and $V(E)$ are the dimensionless forms of the impact-ionization coefficient, recombination coefficient, and drift velocity; their functional forms (see Appendix A) are based on experimental data[36,37] and physical considerations, which are given in Refs. 19, 27, 35, and 38. The compensation ratio α is defined as the ratio of the acceptor concentration to the donor concentration. The dimensionless quantities are defined in terms of dimensional quantities in Table I.[34] The dimensional variables are as follows: $\Phi(t)$ is the voltage bias, X is the distance measured from the injecting contact, t is the time, $\rho_{\rm con}$ is the injecting-contact resistivity, and l is the sample length. In Table II, we state the values of the physical parameters appearing in Table I; they are typical of the high-purity p-type Ge used in experiment.[15,27]

TABLE I. Definition of dimensionless quantities.

Dimensionless quantity	Definition
Spatial variable	$x=X\mu_0 ed/(\epsilon v_s)$
Temporal variable	$\tau=t/t_2$
Electric field	$E(x,\tau)=\mathscr{E}(X,t)\mu_0/v_s$
Voltage bias	$\phi(\tau)=\Phi(t)\mu_0^2 ed/(\epsilon v_s^2)$
Current density	$J(\tau)=j(t)/(edv_s)$
Drift velocity	$V(E)=v_d(\mathscr{E})/v_s$
Impact-ionization coefficient	$K(E)=k(\mathscr{E})/k_0$
Recombination coefficient	$R(E)=r(\mathscr{E})/k_0$
Injecting-contact resistivity	$\rho_0=\rho_{\rm con}e\mu_0 d$
Sample length	$L=l\mu_0 ed/(\epsilon v_s)$

The qualitative nature of much of the predicted behavior—e.g., the instability of the stationary electric-field profile and the stability of propagating high-field domains—depends only on the presence of NNDR,[28,29] and not on the exact form of the underlying coefficients. Other authors have stated different forms of the coefficient curves for various

TABLE II. Physical parameters and time scales used in the analysis and numerical simulation of the Ge system.

Quantity	Value
Donor concentration	$d=8\times10^{10}\ {\rm cm}^{-3}$
Shallow acceptor concentration	$a=9.68\times10^{10}\ {\rm cm}^{-3}$
Compensation ratio	$\alpha\equiv a/d=1.21$
Low-field hole mobility	$\mu_0=1.0\times10^6\ {\rm cm}^2/({\rm V\ s})$
Saturation velocity	$v_s=1.0\times10^7\ {\rm cm/s}$
Permittivity	$\epsilon=16\epsilon_0$
Permittivity of free space	$\epsilon_0=8.85\times10^{-12}\ {\rm C}^2/({\rm N\ m}^2)$
Injecting-contact resistivity	$\rho_{\rm con}=585\Omega\ {\rm cm}$
Lattice temperature	$\mathscr{T}=4.2\ {\rm K}$
Impact-ionization constant	$k_0=6.0\times10^{-6}\ {\rm cm}^3/{\rm s}$
Recombination-ionization constant	$r_0=3.0\times10^{-6}\ {\rm cm}^3/{\rm s}$
Infrared generation constant	$\gamma=1.0\times10^{-4}\ {\rm s}^{-1}$
Diffusivity	$D\equiv\mu_0 k_b\mathscr{T}e=3.6\ {\rm cm}^2/{\rm s}$
Impact-ionization time	$t_2\equiv1/(k_0 d)=2.1\times10^{-6}\ {\rm s}$
Dielectric relaxation time	$t_1\equiv\epsilon/(ed\mu_0)=1.1\times10^{-10}\ {\rm s}$
Sample length	$l=1.45\ {\rm cm}$
Sample cross-sectional area	$A=0.16\ {\rm cm}^2$
Elementary charge	$e=1.602\times10^{-19}\ {\rm C}$

reasons.[39–41] Recently, Monte Carlo simulation has been used to provide a more rigorous determination of the coefficients for a related p-type system;[42] however, such simulations do not yet exist for the Ge samples under consideration in this paper.

Equation (1a) is first order in the spatial variable x, so we may only specify one boundary condition. We choose to satisfy an Ohmic boundary condition at the injecting contact. Although p-type Ge experiments have two Ohmic contacts,[15] only the injecting contact should be important in determining the behavior in the bulk;[28,34,43] therefore, we neglect the receiving-contact boundary condition. This produces unphysical results in a narrow diffusive layer near the receiving contact (thickness $\sim 0.5\ \mu$m); we have treated this effect elsewhere.[28] In addition to the injecting boundary condition, we also have a global voltage-bias constraint. The dimensionless boundary condition and voltage constraint for Eq. (1a) are

$$E(x=0,\tau)=\rho_0 J(\tau), \quad \int_0^L E(x,\tau)dx=\phi(\tau). \tag{2}$$

III. DYNAMICS UNDER dc+ac VOLTAGE BIAS

The case of pure dc bias has been treated in detail elsewhere;[19,28,29,31,33] we will summarize briefly the main results. As the voltage is increased beyond the value for impurity breakdown, the stationary state loses stability to small-amplitude (SA) periodic oscillations via a Hopf bifurcation. This bifurcation occurs at a voltage we define as Φ_α, $\Phi_\alpha/l \approx 6.046$ V/cm. The SA current oscillations are composed of a very sinusoidal component (~ 0.01 mA) offset by a larger dc component (~ 1.0 mA). The current oscillations result from dipole charge waves that nucleate at the injecting contact and quickly decay as they detach from the contact. At a larger voltage, Φ_β ($\Phi_\beta/l \approx 6.055$ V/cm), the system undergoes an abrupt hysteretic transition from the SA oscillations to large-amplitude (LA) periodic oscillations. The LA current oscillations are composed of a wave train of pulses (~ 0.1 mA) offset again by a larger dc component (~ 1.0 mA). The LA current oscillations result from the periodic nucleation of electric-field solitary waves that propagate across the entire sample. The frequencies of the oscillations are ~ 3.0 kHz for the SA oscillations and ~ 0.5 kHz for the LA oscillations. The periodic oscillations persist until the voltage becomes larger than a value, Φ_ω ($\Phi_\omega/l \approx 12.975$ V/cm), beyond which the stationary state is again stable.

Here we add a small sinusoidal component to the dc bias, so that the total bias is

$$\Phi(t)/l=\mathscr{E}_{\rm dc}+\mathscr{E}_{\rm ac}\sin(2\pi f_{\rm dr}t), \tag{3}$$

where $\mathscr{E}_{\rm ac}$ ($\mathscr{E}_{\rm dc}$) is the ac (dc) amplitude and $f_{\rm dr}$ is the drive frequency of the ac signal. There are two natural frequencies of the system, the drive frequency and the frequency of the spontaneous periodic oscillation f_0 associated with the pure dc-bias case. For the ac results reported here, we have set $\mathscr{E}_{\rm dc}=7.5V/{\rm cm}$ in order to closely mimic the experimental conditions of Kahn, Mar, and Westervelt.[22,23] The frequency of the spontaneous oscillation in our model for $\mathscr{E}_{\rm dc}=7.5$V/cm is $f_0=0.77$ kHz. The ac drive and the spontaneous oscillation of the sample can be thought of as two oscillators interacting in a nonlinear medium. For such a system, we would expect different dynamical behavior depending on the drive parameters. Kahn, Mar, and Westervelt observe frequency locking, quasiperiodicity, temporal chaos, and spatiotemporal chaos in their system.[22,23] Gwinn and Westervelt find that the dynamics is consistent with the circle-map model of the quasiperiodic transition to chaos.[44,45] Recently, Jiang[46] employed a two-Fourier-mode space-charge dipole decomposition of Teitsworth and Westervelt's rate equations[26,27] (neglecting carrier population dynamics). He finds frequency locking, quasiperiodicity, and chaos under dc+ac bias. In our simulations we find frequency locking and quasiperiodicity, but not chaotic behavior.

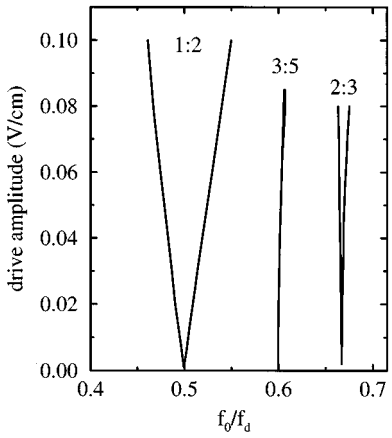

FIG. 2. Tongue diagram. Inside the tongues the response frequency is locked to the drive frequency with the indicated ratio.

The tongue diagram (Fig. 2) shows the regions of drive bias and frequency where the current oscillations are synchronized to a rational multiple of the drive frequency. Outside of the tongue regions the system is quasiperiodic. The tongues are constructed by observing the Poincaré section map formed by sampling the current time series at multiples of the drive period. The tongues widths increase with drive amplitude and eventually overlap at the critical line. In determining the critical line, we use the fact that overlapping tongues produce hysteretic boundaries.[44] We place the upper limit of the tongues at the critical line, i.e., where we first observe hysteretic behavior. We find that the critical line in our model occurs at roughly 1/3 the drive amplitude of the critical line in the experimental system.[22] This is an indication that our model system locks more readily to the drive signal than does the experimental system.

Above the critical line in the circle-map model, chaotic behavior is possible.[47] Kahn, Mar, and Westervelt observe both temporal and spatiotemporal chaos in the system above the critical line.[23] We do not observe chaos in our numerical simulations, but we do see spectrally rich quasiperiodicity above the critical line, as shown in Fig. 3(a). Kahn, Mar, and Westervelt observe spatiotemporal chaos when they drive the system with an ac drive voltage large enough to cause the voltage bias to go below the onset value for spontaneous oscillations Φ_α.[23] In such cases, they observe the nucleation and destruction of domains in the bulk of the sample, rather

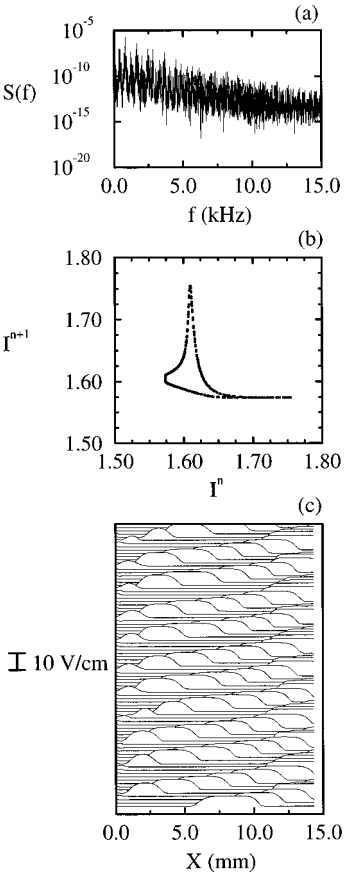

FIG. 3. (a) The Fourier power spectrum vs frequency, (b) the Poincaré section map (system strobed at $1/f_d$), and (c) $\mathscr{E}(X,t)$ at intervals of 0.16 ms for $\mathscr{E}_{\rm dc}=7.5$ V/cm, $\mathscr{E}_{\rm ac}=0.25$ V/cm, and $f_d=1.18$ kHz ($f_0/f_d=0.65$).

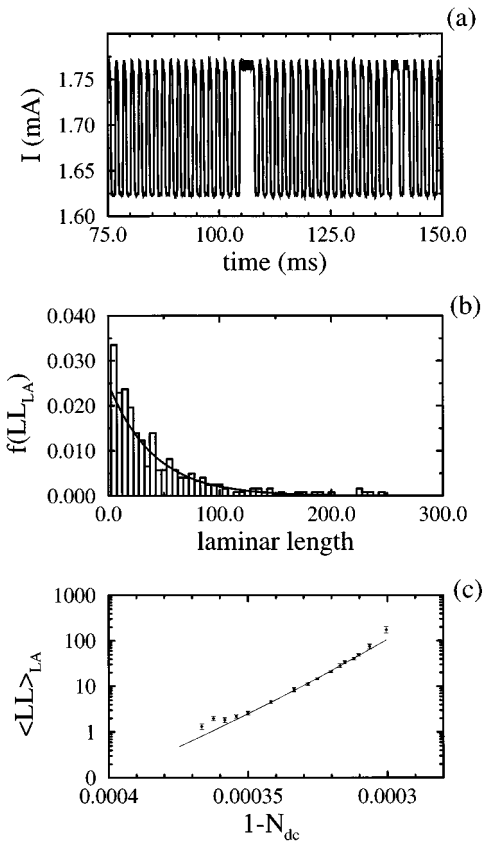

FIG. 4. (a) Current showing intermittent switching between small-amplitude and large-amplitude oscillations for $\eta=0.002$ V/cm and $\mathscr{E}_{\rm dc}=6.055\,38$V/cm. (b) The laminar-length probability-density distribution for the same bias and noise strength as in (a) (the solid line is the predicted distribution function). (c) The average laminar length vs the distance $\mathscr{E}_{\rm dc}$ is from $\mathscr{E}_{\rm crit}$; the solid line is the fitted power law, and the vertical bars correspond to 1 standard deviation of the mean (each data point is the average result from many time series).

than domains being solely nucleated at the injecting contact and being destroyed only at the receiving contact. In contrast, we observe nucleation only at the injecting contact for a spatially constant compensation profile. When we apply an ac signal that drives $\Phi(t)$ below Φ_α the domains are destroyed in the bulk, but the new domains are always nucleated at the injecting contact as Φ rises through Φ_α. This forces the sample oscillation into a 1:1 locking with the drive frequency.

There are several possible reasons that our simulations do not capture the chaotic dynamics reported in experiment. One cause, a spatially varying compensation profile, will be discussed in Sec. V. Also, there is the possibility that the terms ignored in the reduced equation—namely, the diffusion and displacement currents—are important in the chaotic regime.

IV. NOISE-INDUCED INTERMITTENT SWITCHING

In this section we explore how the addition of a small noise term to the voltage bias results in the intermittent switching of the system between the LA and SA states for voltages near Φ_β. Under pure dc bias, there is a hysteretic bifurcation from the SA oscillation state to the LA solitary-wave state at Φ_β, with no intermittent switching.[19,29,33] By adding a small Gaussian δ-correlated noise term to the dc bias we find that the current exhibits intermittent switching between the SA state and the LA state for biases near Φ_β; see Fig. 4(a).

The intermittent switching in our model does share common traits with other types of intermittent behavior, but does not fit into any particular classification. For instance, in a pulse-modulated (PM) transition the system randomly alternates between a periodic (laminar) state and a chaotic state.[48,49] An important point is that PM-type intermittency occurs for fixed system parameters near the bifurcation from periodic to chaotic behavior, whereas our intermittent switching is noise induced. Also, both states (SA and LA) between which our system switches are regular; the intermittent switching is a continuous route from the periodic SA state to the periodic LA solitary-wave state, rather than from a periodic state to a chaotic state. Like PM-type intermittency, the average time the system spends in one state scales as a power law with the ''distance'' from the bifurcation point.

Recently, there has been a great deal of interest in systems where a control parameter is driven by noise through a bifurcation point, resulting in the system switching between

two states. This phenomenon has been labeled by Platt, Spiegel, and Tresser as "on-off intermittency"[50] and has been observed in systems of ordinary differential equations,[50] maps,[51] coupled-map lattice systems,[52] and nonlinear electronic circuits.[53,54] Although on-off intermittency is also noise driven, its statistical properties differ from those of our model.

With the addition of a noise term the time-discretized bias is given by

$$\Phi^j/l = \mathscr{E}_{\rm dc} + \eta\xi^j, \tag{4}$$

where ξ^j satisfies

$$\langle \xi^j \rangle = 0, \langle \xi^j \xi^m \rangle = \delta_{jm}. \tag{5}$$

The superscripts j and m are indices for the discretized time and $\langle\rangle$ denotes $(1/n)\Sigma_{j=1}^{n}$, n being the total number of time steps. For all the results stated here, ξ is an uncorrelated Gaussian-distributed random variable with a variance of 1.0. The noise strength η is scaled as the inverse square root of our discrete time step $\Delta\tau$ so that in the limit of continuous time $(\Delta\tau \to 0)$ the noise becomes δ-correlated $\langle \xi(\tau)\xi(\tau+T)\rangle = \delta(T)$. In our simulations, $\Delta\tau = 0.5$, and correspondingly $\eta \equiv (0.001\ 414 \text{V/cm})/\sqrt{\Delta\tau} = 0.002\ \text{V/cm}$, which we estimate to be of the same order of magnitude as the noise in the experimental bias.[24,55]

The two spatially averaged electric-field values (Φ/l) that delimit the hysteretic region, $\mathscr{E}_{\alpha_1}$ and $\mathscr{E}_{\alpha_2}$, are important in the analysis of the switching statistics. The hysteretic region extends from $\mathscr{E}_{\alpha_1} \approx 6.0551$ V/cm to $\mathscr{E}_{\alpha_2} \approx 6.0554$ V/cm. For $\Phi_\alpha/l < \mathscr{E}_{\rm dc} < (\mathscr{E}_{\alpha_1} - \eta)$, the current is essentially in the SA state; as $\mathscr{E}_{\rm dc}$ increases to $\mathscr{E}_{\alpha_1}$, the SA oscillations become interrupted by regions of LA oscillations. As the bias is further increased, the temporal length of the LA oscillations grows, until for biases $(\mathscr{E}_{\alpha_2} + \eta) < \mathscr{E}_{\rm dc} < \Phi_\omega/l$, the system has asymptotically zero probability of leaving the LA state. We call the regions of LA oscillations laminar regions in order to be consistent with the analysis of Kahn, Mar, and Westervelt[24] and to facilitate comparison of our results with other types of intermittency (e.g., type-III intermittency and on-off intermittency).

For the noise to change the state of the system (SA $\leftrightarrow$ LA), we find that it must cause the bias to leave the hysteretic region for a time longer than the nucleation time for a pulse of the other state.[56] For example, assume that the system is in the LA state. For the system to switch to the SA state the noise must shift the bias so that $\Phi/\text{l} < \mathscr{E}_{\alpha_1}$ for a time long enough to nucleate a SA pulse. Let the number of consecutive discrete time steps corresponding to the nucleation time for a SA pulse be given by ν_1. For a small noise amplitude (as used here), we find that the LA state is unstable only to the SA state for a period of time during the nucleation of a solitary wave; when a solitary wave is propagating in the bulk the LA state is robust against the noise and SA pulses are never nucleated.[56] Let ν_2 be the number of discrete time steps per LA oscillation period during which the LA oscillation is susceptible to the nucleation of a SA pulse for a given noise strength. Assuming that the system is in the LA state, the probability for completing one LA cycle without nucleating a SA pulse is

$$P_{\rm LA} = 1 - P_{\rm SA}, \tag{6}$$

where

$$P_{\rm SA} = \left\{ 1 - (\nu_2 - \nu_1 + 1)\left[\int_{\Delta\mathscr{E}}^{\infty} \frac{1}{\eta\sqrt{2\pi}} \exp\left(\frac{-x^2}{2\eta^2} \right) dx \right]^{\nu_1} \right\} \tag{7}$$

is the probability of nucleating a SA pulse during one LA period and $\Delta\mathscr{E} = (\mathscr{E}_{\rm dc} - \mathscr{E}_{\alpha_1})$. The factor $[]^{\nu_1}$ is the probability of the Gaussian noise resulting in $\Phi/l < \mathscr{E}_{\alpha_1}$ for ν_1 consecutive steps. The term $(\nu_2 - \nu_1 + 1)$ is the number of ways a consecutive interval of discrete steps of length ν_1 can appear in an interval of length ν_2. The laminar length (LL) of a wave train of oscillations is defined as the number of consecutive periodic cycles completed in a given state (either SA or LA). The probability of observing a laminar length y for the LA state is proportional to $P_{\rm LA}^{y} P_{\rm SA}$, and after normalization leads to a probability density function,

$$f(y) = -(1 - P_{\rm SA})^{y} \ln(1 - P_{\rm SA}). \tag{8}$$

The average laminar length of the LA oscillations $\langle\ \text{LL}\ \rangle_{\rm LA}$ is given by

$$\langle \text{LL} \rangle_{\rm LA} = \int_0^{\infty} f(y)\, y\, dy \tag{9}$$

$$= \frac{-1}{\ln(1 - P_{\rm SA})} \tag{10}$$

$$\approx \frac{1}{P_{\rm SA}} \tag{11}$$

$$\propto \frac{1}{\left[\text{erf}\left(\dfrac{\Delta E}{\eta\sqrt{2}} \right) \right]^{\nu_1}}. \tag{12}$$

We selected our range of biases, $\mathscr{E}_{\alpha_1} \lesssim \mathscr{E}_{\rm dc} \lesssim \mathscr{E}_{\alpha_2}$, so that the range of $\langle\ \text{LL}\rangle_{\rm LA}$ encompasses those observed by Kahn, Mar, and Westervelt[24] and such that we can obtain reasonable statistics for the laminar-length distribution with our available computer resources. For the above range of biases, we have $\Delta\mathscr{E}/\eta \approx 1/10$; so we may use the small number expansion of the complimentary error function, and arrive at the following proportionality:

$$\langle \text{LL} \rangle_{\rm LA} \propto \left(\eta\sqrt{\frac{\pi}{2}} + \mathscr{E}_{\alpha_1} - \mathscr{E}_{\rm dc} \right)^{-\nu_1}. \tag{13}$$

We define $\mathscr{E}_c \equiv (\eta\sqrt{\pi/2} + \mathscr{E}_{\alpha_1}) \approx 6.0575$ V/cm and arrive at a power-law scaling for the average laminar length for biases $|\Delta\mathscr{E}/\eta| < 1$. For biases larger than those in our selected range, we expect $\langle\ \text{LL}\ \rangle_{\rm LA}$ to continue to increase, but that our power-law result, Eq. (12), may become invalid. As $|\Delta\mathscr{E}/\eta|$ increases to 1, the small number expansion of erf fails. In the limit of $|\Delta\mathscr{E}/\eta| \gg 1$, $\langle\ \text{LL}\ \rangle_{\rm LA}$ will diverge as a modified Gaussian; therefore, only for biases in the range approximated by $(\mathscr{E}_{\alpha_1} - \eta) < \mathscr{E}_{\rm dc} < (\mathscr{E}_{\alpha_1} + \eta)$ would we expect to see a power-law scaling.

We also expect the functional dependence of the average laminar lengths on $\mathscr{E}_{\rm dc}$ to change as $\mathscr{E}_{\rm dc}$ leaves the hysteretic region. Consider the following situation: for $\mathscr{E}_{\rm dc}=(\mathscr{E}_{\alpha_1}-\epsilon)$ ($\epsilon\equiv$ arbitrarily small field value) the probability of obtaining a $\langle\,{\rm LL}\,\rangle_{\rm LA}$ of greater than one is fundamentally different than for $\mathscr{E}_{\rm dc}=(\mathscr{E}_{\alpha_1}+\epsilon)$. This is because as $\mathscr{E}_{\rm dc}$ passes through $\mathscr{E}_{\alpha_1}$ in a noiseless system the LA state changes from an unconditionally unstable state to a conditionally stable state (i.e., the system is hysteretic). In contrast, as $\mathscr{E}_{\rm dc}$ is increased past $\mathscr{E}_{\alpha_2}$ the functional form of $\langle\,{\rm LL}\,\rangle_{\rm LA}$ should not change since the LA state remains a stable state of the system, but we expect the shape of the $\langle\,{\rm LL}\,\rangle_{\rm SA}$ curve to change due to the loss of stability of the SA state. In this manner, we expect to see two regions of different functional behavior for $\langle\,{\rm LL}\,\rangle_{\rm LA}$, one for $\mathscr{E}_{\rm dc}<\mathscr{E}_{\alpha_1}$ and another for $\mathscr{E}_{\rm dc}>\mathscr{E}_{\alpha_1}$.

Kahn, Mar, and Westervelt[24] find intermittent switching near the onset of solitary-wave-mediated oscillations. The statistics of their intermittency are consistent with PM type-III intermittency. The wave forms they observe are different from those we see in Fig. 4(a). The SA oscillations in the experiments of Kahn, Mar, and Westervelt are noisy and are suppressed after a region of LA spikes, whereas our SA oscillations are very regular and recover instantly after a LA laminar region. Also, their LA oscillations have a more irregular wave form than the uniform LA oscillations in our simulations. This may indicate that our assumed noise strength is below the level appropriate to the experimental system.

The numerical simulations support our analytic predictions for the probability-density distribution and the power-law scaling of the average laminar lengths. The probability-density distribution of LA laminar lengths for $\mathscr{E}_{\rm dc}=6.055\,38V/{\rm cm}$ is show in Fig. 4(b). The histogram has bins of width 5.0 and is normalized so that the area under the histogram is equal to 1.0. We used 266 laminar regions to construct the histogram. The solid line in Fig. 4(b) is $P^{y}_{\rm LA}P_{\rm SA}$, where we have used Eq. (11) to determine $P_{\rm SA}$ from simulation result $\langle\,{\rm LL}\,\rangle_{\rm LA}\approx 40.7$ for $\mathscr{E}_{\rm dc}=6.055\,38V/{\rm cm}$. We then normalized the distribution so that the area under the curve equals 1.0 over the domain of the histogram. The numerics are consistent with the predictions considering the limited number of laminar regions used to construct the histogram. We perform an error-weighted nonlinear least-squares fit of the average laminar lengths to $C\cdot(\mathscr{E}_{\rm crit}-\mathscr{E}_{\rm dc})^{\theta}$, where C is the proportionality constant in Eq. (13). We use only the data $\mathscr{E}_{\rm dc}>\mathscr{E}_{\alpha_1}$—we ignore the data $\mathscr{E}_{\rm dc}<\mathscr{E}_{\alpha_1}$ because there is a change in the functional behavior of $\langle\,{\rm LL}\,\rangle_{\rm LA}$ at $\mathscr{E}_{\rm dc}=\mathscr{E}_{\alpha_1}$. We find from the fit that $\mathscr{E}_{\rm crit}=6.0572{\rm V/cm}$, which is in good agreement with the analytic prediction of Eq. (13) that $\mathscr{E}_{c}\approx 6.0575\ {\rm V/cm}$. The fit also produces $\theta=-24.35$. Kahn, Mar, and Westervlet find $\theta=-0.85$ and $\mathscr{E}_{\rm crit}\approx 6.3\ {\rm V/cm}$.[24] Our result $\theta=-24.35$ indicates that the bias must be below $\mathscr{E}_{\alpha_1}$ for approximately 24 consecutive time steps before a SA pulse is nucleated from a LA state; in contrast, the experimental result indicates that a single step below $\mathscr{E}_{\alpha_1}$ should nucleate a SA pulse. The observed $\langle\,{\rm LL}\,\rangle_{\rm LA}$ and the fitted power law are shown in Fig. 4(c), where we have defined $(1-\epsilon_{\rm dc})\equiv(\mathscr{E}_{\rm crit}-\mathscr{E}_{\rm dc})/\mathscr{E}_{\rm crit}$.

Although our simple attempt at including noise in the model system produces results that do not agree quantitatively with experiment, it does illustrate the potential for noise as a source of switching behavior. The sensitivity of our model system to noise during nucleation also fits well with Kahn, Mar, and Westervelt's observations that during nucleation fluctuations in the electric-field profile are enhanced.[15] Rather than adding external noise to the voltage bias, we could model the noise more realistically as spatially distributed fluctuations in the electric field. The noise would correspond to fluctuations in the carrier velocity due to thermal effects and to fluctuations in the free hole concentration due to generation and recombination $(g-r)$ processes.[42,57] Kuhn *et al.*[42] have performed a Monte Carlo study of the noise processes in cooled p-type Ge. They find that the g-r processes are the principal source of noise for electric-field values in our range of interest. They find enhanced noise levels for biases near the impurity breakdown value and observe bias-dependent high-frequency cutoffs of their Lorentzian noise spectra that approach 0.1 MHz, which corresponds to a noise source that fluctuates on a time scale ten times longer than the one we used in our simulations. Although their results are not directly applicable to our system due to the different donor ($10^{12}\ {\rm cm}^{-3}$ and $10^{13}\ {\rm cm}^{-3}$) and acceptor ($10^{14}\ {\rm cm}^{-3}$) concentrations, their method of calculating the $g-r$ noise could be used in future simulations.

By using a noise spectrum such as Kuhn's, with a lower high-frequency cutoff, and by using a spatially distributed noise source, the statistics of the intermittent switching may become more like those found in type-III and on-off intermittency. In particular, both type-III and on-off intermittency have probability distributions for the laminar lengths that scale as $({\rm LL})^{3/2}$ for short laminar lengths and decay exponentially for long lengths.[48,51] Also in both types of intermittency, the average laminar length scales as Δ^{-1}, where Δ is the distance of the bifurcation parameter from the onset value [in our case Δ corresponds to $(\mathscr{E}_{\rm crit}-\mathscr{E}_{\rm dc})$].[48,51] If such statistics were found in our model, it would be (to our knowledge) the first partial-differential-equation model of a spatially extended continuum system to show on-off intermittency.

V. SPATIALLY-VARYING COMPENSATION RATIO

Our model system is very sensitive to spatial variations in the compensation ratio $\alpha(X)$. A variation in the compensation profile changes the local $j_{\rm sh}(\mathscr{E})$ relationship[19] and causes the voltage associated with a solitary wave (the domain voltage) to change as the domain propagates across the sample. The wave form of the current is determined by the domain voltage. Following Kahn *et al.*, we consider the sample divided into two distinct regions: the region occupied by the solitary wave and the region outside of the solitary wave.[24] The sum of the voltages of these two regions must equal the voltage bias, and results in a smaller domain voltage producing a larger current. This is because in the region outside the domain the electric field is in the positive differential resistance region of the $j_{\rm sh}(\mathscr{E})$ curve, and in order to increase the voltage falling across this region (in order to compensate for the smaller domain voltage) the current must increase correspondingly. We expect therefore that a varia-

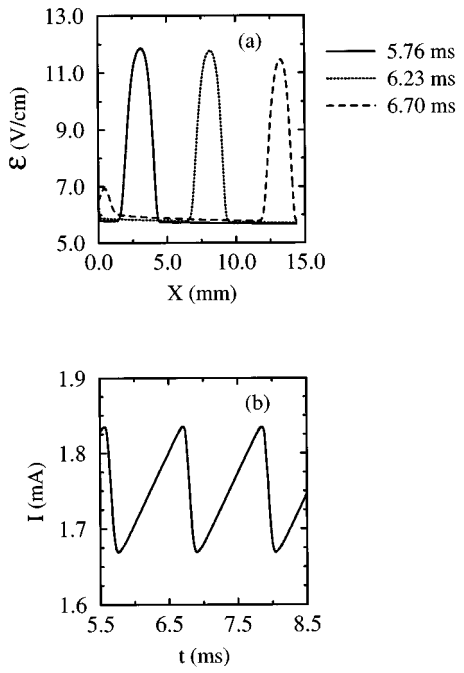

FIG. 5. (a) $\mathscr{E}(X,t)$ as a domain propagates across the sample with a linearly increasing compensation ratio, $\alpha(X)=1.21+0.015(X/l)$, and $\mathscr{E}_{dc}=6.5$ V/cm. (b) The corresponding current wave form.

tion in the compensation ratio will affect the wave form of the current; a decreasing/increasing domain voltage will cause the current to increase/decrease simultaneously. We take advantage of this relationship between the spatial profile of the compensation ratio and the spatiotemporal dynamics of the system to create behavior that is more consistent with experiment. In particular, by selecting a linearly increasing compensation profile we are able to produce sawtooth current wave forms and decaying solitary waves that are similar to the experimental results of Kahn *et al.*[15]

We expect smaller solitary waves for larger values of α due to the decreased range of electric-field values that display NDR.[31,34] In fact, for $\alpha>1.825$, NDR is not present in $j_{sh}(\mathscr{E})$,[19] and the system does not support solitary waves. In Fig. 5(a) and Fig. 5(b), the electric-field profile and current are shown for $\alpha(X)=1.21+0.015(X/l)$ with $\mathscr{E}_{dc}=6.5$ V/cm. For biases $5.9\text{ V/cm}\lesssim\mathscr{E}_{dc}\lesssim 8.0\text{V/cm}$, the current wave forms have a sawtooth shape, but at higher biases the wave forms are qualitatively different due to the simultaneous presence of two solitary waves, one near the injecting contact and one leaving the sample. The above $\alpha(X)$ profile is consistent with the Czochralski growth method and the zone refining technique used in the fabrication of the samples,[15] where the different segregation coefficients of the impurities may cause a spatial variation in the compensation ratio.[58] The profile of the compensation ratio for the crystal used in the experiments of Kahn *et al.* is not known to the 1.0% accuracy necessary in our simulations,[59] so we have chosen a linear profile as a simple model that improves the agreement between our simulations and experimental observations.

The linearly-increasing compensation ratio produces an asymmetric dependency on the polarity of the bias and also produces a continuous nonhysteretic transition from the small-amplitude oscillatory state to the large-amplitude oscillatory state. Under reverse bias for the same contact resistance, the current oscillations occur over a much smaller bias range, $10.5\text{ V/cm}<\mathscr{E}_{dc}<13.25\text{V/cm}$, but have approximately the same amplitude as the forward biased oscillations. Kahn, Mar, and Westervelt[15] find that the experimental system is also asymmetric; the current oscillations are larger and less noisy for a particular bias polarity. In contrast to our results, they find that the onset bias to oscillatory behavior is approximately the same for both polarities. There are at least two possible reasons for the disagreement between the experimental and simulated reverse-bias results; the compensation profile could be more complicated than our simple linear model or the receiving and injecting contacts could have different resistivity values. We find that both the compensation profile and the contact resistivity have dramatic effects on the behavior of the system, so that by ''tuning'' both we could likely reproduce the experimental results. In previous numerical simulations,[19,29,33] we showed that there is an abrupt hysteretic jump from the small-amplitude decaying-wave state to the large-amplitude solitary wave state in a system with a constant compensation profile. In the system with the above $\alpha(X)$ profile, there is no longer a jump but rather as the bias is increased, the decaying waves grow in amplitude and penetrate further into the sample, until for a large enough bias, they reach the receiving contact. Upon reaching the contact, the solitary wave is destroyed and a new wave is nucleated at the injecting contact in the same manner that periodic solitary waves were generated in the uniform α system. The gradual increase in the amplitude and penetration depth produces a continuous decrease in the frequency and an increase in the magnitude of the current oscillations.

VI. CONCLUSIONS

The simplest form of our model—for a uniform compensation profile and a noise-free voltage bias—captures only some aspects of the experimental system. We find frequency locking and quasiperiodic behavior under dc+ac bias, although the critical line occurs at biases approximately a factor of 3 smaller than the experimental values.[23] In order to produce intermittent switching, we add a small δ-correlated noise term to the bias. The small noise term does not perturb the gross features of the system, but it does cause intermittent switching between the SA and LA states for biases close to the hysteretic transition region. The statistics of the intermittent switching differ from those found in PM type-III and on-off intermittency, but we speculate that a spatially distributed noise term with a reduced high-frequency cutoff value could produce statistics that are more similar.

Also, the experimentally observed solitary waves decrease in amplitude as they propagate, whereas the solitary waves we generate for a spatially uniform compensation ratio have constant amplitude as they propagate across the sample. By adding a small, linearly increasing term to the constant compensation ratio we produce solitary waves that shrink as they propagate across the sample. Furthermore, the addition of a small, spatially-random component to $\alpha(X)$

causes small variations in the domain voltage as the domain propagates across the sample. The variation in domain voltage causes a scalloping of the current wave form that is reminiscent of the current wave forms observed in experiment.[15] Spatial variation of the compensation profile might also be necessary for chaotic behavior. As stated in Sec. III, for a constant profile we find that our system does not support chaotic behavior, but preliminary numerical results indicate that under dc+ac bias, a system with a small random component in $\alpha(X)$ can be driven chaotic.[56]

ACKNOWLEDGMENTS

It is a pleasure to acknowledge beneficial conversations with E. E. Haller, A. M. Kahn, and D. J. Mar. We acknowledge financial support from the National Science Foundation through Grant No. DMR-9157539, the Spanish DGICYT through Grant No. PB92-0248, and the NATO Travel Grant Program through Grant No. CRG-900284.

APPENDIX A: COEFFICIENT FUNCTIONS

The phenomenological forms of the recombination coefficient, $r(E)$, impact-ionization coefficient, $k(E)$, and drift velocity, $v_d(E)$, are stated here in terms of the dimensionless electric field, E:

$$v_d(E)=v_s\left\{0.9(E+0.33)+\frac{1.8}{\pi}(E-0.5)\tan^{-1}(5.0-10.0E)+\frac{0.09}{\pi}\ln[1.0+(5.0-10.0E)^2]\right\}, \tag{A1}$$

$$r(E)=r_0\{0.05+(1.04+100.0E^2)^{-1.5}\}, \tag{A2}$$

$$k(E)=k_0\left\{\left[1.0+\exp\left(\frac{0.55-E}{0.015}\right)\right]^{-1}\left[0.25+2.0\exp\left(\frac{-E}{0.34}\right)\right]+0.1\left(\frac{E}{1.15}\right)^4\right\}. \tag{A3}$$

APPENDIX B: NUMERICAL ALGORITHM

We use a second-order upwind finite-difference approximation to the spatial derivatives, and advance the solution in time with a second-order Runge-Kutta method. The hyperbolic nature of the partial differential equation (PDE) necessitates upwind differencing in order to obtain numerical stability.[43] The injecting-contact boundary condition and global voltage constraint, along with the discretized PDE forms a doubly bordered band matrix. We arrange the matrix system so that it is efficiently solved using standard LINPACK direct matrix solving routines.

We discretize Eq. (1a) by using the following approximations to the derivatives (in dimensionless units):

$$\left(\frac{dE}{dx}\right)_i^k=\frac{3E_i^k-4E_{i-1}^k+E_{i-2}^k}{2\Delta x}+O(\Delta x^2), \tag{B1}$$

$$\left(\frac{dE}{d\tau}\right)_i^k=\frac{E_i^{k+1}-E_i^k}{\Delta\tau}+O(\Delta\tau), \tag{B2}$$

where the k and i indicate discrete points in time and space, respectively. The spatial grid spacing is Δx, and $\Delta\tau$ is the temporal step size. We discretize the problem on a spatial grid with $(N+1)$ points $[0,N]$, and start from a uniform initial field, $[E_i^{k=0}]=\phi^{k=0}/L$. We solve the discretized problem to machine precision on the interior N points, subject to an Ohmic boundary condition on the injecting contact. The global boundary constraint is the $(N+1)$ equation—which we evaluate using the trapezoid rule—and it completes the set of equations that uniquely specifies our electric field on the grid. The quasilinear nature of Eq. (1a) allows a simple explicit matrix formulation of the problem. By approximating the temporal derivatives with Eq. (18) and evaluating the coefficients, $c_1(E,J)$, $c_2(E,J)$, and $c_3(E,J)$ and $V(E)$ at the discrete time step, k, we explicitly advance the electric field to first order in time by solving the following eigenvalue problem:

$$A\mathbf{E}=\mathbf{b}. \tag{B3}$$

The components of the matrix A and the vector $\mathbf{b}$ depend only on E_i^k. The vector $\mathbf{E}$ contains the elements $[E_i^{k+1}]_{i=0}^N$. The matrix A has a doubly bordered band-matrix form,

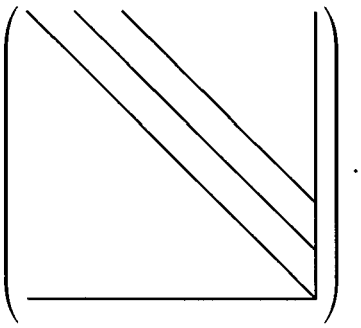

We block decompose the system so that we can use a standard band matrix solver. We identify $T,\mathbf{v},\mathbf{u},\mathbf{x},\mathbf{s},a_{11},\mu$, and s_1 from Eq. (B3),

$$\begin{pmatrix}(T)&(v)\\(u)&(a_{11})\end{pmatrix}\begin{pmatrix}(x)\\(\mu)\end{pmatrix}=\begin{pmatrix}(s)\\(s_1)\end{pmatrix}. \tag{B4}$$

We solve for two vectors, $\mathbf{y}$ and $\mathbf{z}$, defined by

$$T\mathbf{y}=\mathbf{s},\quad T\mathbf{z}=\mathbf{v}. \tag{B5}$$

We have from Eq. (B4)

$$a_{11}\mu+\mathbf{u}\cdot\mathbf{x}=s_1, \tag{B6}$$

$$\mu\mathbf{v}+T\mathbf{x}=\mathbf{s}. \tag{B7}$$

Equation (B5) with Eqs. (B6) and (B7) give

$$\mathbf{y}=\mu\mathbf{z}+\mathbf{x}, \tag{B8}$$

$$\mu=\frac{s_1-\mathbf{u}\cdot\mathbf{x}}{a_{11}}. \tag{B9}$$

Using Eq. (B8) to eliminate $\mathbf{x}$ from Eq. (B9) yields the solution for μ,

$$\mu = \frac{s_1 - \mathbf{u}\cdot\mathbf{y}}{a_{11} - \mathbf{u}\cdot\mathbf{z}}. \tag{B10}$$

The rest of the electric-field values, **x**, are then specified by Eq. (24). This solves the system to first order in time. We use the first-order advanced field values in a second-order Runge-Kutta (improved tangent) approximation to obtain field values that are second order accurate in time.[60] This results in the final order of the advance field being $O(\Delta x^2, \Delta \tau^2)$.

*Electronic address: mjb@phy.duke.edu
†Electronic address: teitso@phy.duke.edu
‡Electronic address: bonilla@ing.uc3m.es
§Electronic address: drodriguez@etseccpb.upc.es

[1] S. W. Teitsworth, R. M. Westervelt, and E. E. Haller, Phys. Rev. Lett. **51**, 825 (1983).
[2] J. Peinke, A. Muhlbach, R. P. Huebuer, and J. Parisi, Phys. Lett. **108A**, 407 (1985).
[3] K. Aoki, K. Miyamae, T. Kobayahi, and K. Yamamoto, Physica **117B&118B**, 570 (1983).
[4] B. K. Ridley and R. G. Pratt, J. Phys. Chem. Solids **26**, 21 (1965).
[5] C. Hilsum, Proc. IRE **50**, 185 (1962).
[6] J. B. Gunn, IBM J. Res. Dev. **8**, 141 (1964).
[7] K. Hess, H. Morkoc, H. Schichijo, and B. G. Streetman, Appl. Phys. Lett. **35**, 469 (1979).
[8] M. Keever *et al.*, Appl. Phys. Lett. **38**, 36 (1981).
[9] L. L. Bonilla *et al.*, Phys. Rev. B **50**, 8644 (1994).
[10] F. Prengel, A. Wacker, and E. Schöll, Phys. Rev. B **50**, 1705 (1994).
[11] E. Schöll, *Nonequilibrim Phase Transitions in Semiconductors*, Springer Series in Synergetics Vol. 35 (Springer-Verlag, Berlin, 1987).
[12] E. Schöll, in *Nonlinear Dynamics in Solids*, edited by H. Thomas (Springer-Verlag, Berlin, 1992), pp. 31–50.
[13] M. C. Cross and P. C. Hohenberg, Rev. Mod. Phys. **65**, 851 (1993).
[14] R. Döttling and E. Schöll, Solid State Electron. **37**, 685 (1994).
[15] A. M. Kahn, D. J. Mar, and R. M. Westervelt, Phys. Rev. B **43**, 9740 (1991).
[16] M. P. Shaw, V. V. Mitin, E. Schöll, and H. L. Grubin, *The Physics of Instabilities in Solid State Electron Devices* (Plenum Press, New York, 1992).
[17] D. G. Seiler, C. L. Littler, R. J. Justice, and P. W. Milonni, Phys. Lett. **108A**, 462 (1985).
[18] K. Jamada *et al.*, Solid State Electron. **31**, 809 (1988).
[19] S. W. Teitsworth, M. J. Bergmann, and L. L. Bonilla, in *Nonlinear Dynamics and Pattern Formation in Semiconductors and Devices*, edited by F.-J. Niedernostheide, Springer Proceedings in Physics Vol. 79 (Springer-Verlag, Berlin, 1995), pp. 46–69.
[20] S. W. Teitsworth and R. M. Westervelt, Physica D **23**, 181 (1986).
[21] J. Peinke, D. B. Schmid, B. Röricht, and J. Parisi, Z. Phys. B **66**, 165 (1987).
[22] A. M. Kahn, D. J. Mar, and R. M. Westervelt, Phys. Rev. Lett. **46**, 369 (1992).
[23] A. M. Kahn, D. J. Mar, and R. M. Westervelt, Phys. Rev. B **46**, 7469 (1992).
[24] A. M. Kahn, D. J. Mar, and R. M. Westervelt, Phys. Rev. B **45**, 8342 (1992).
[25] J. Peinke *et al.*, Appl. Phys. A **48**, 155 (1989).
[26] S. W. Teitsworth and R. M. Westervelt, Phys. Rev. Lett. **53**, 2587 (1984).
[27] R. M. Westervelt and S. W. Teitsworth, J. Appl. Phys. **57**, 5457 (1985).
[28] L. L. Bonilla, Phys. Rev. B **45**, 11 642 (1992).
[29] L. L. Bonilla, I. R. Cantalapiedra, M. J. Bergmann, and S. W. Teitsworth, Semicond. Sci. Technol. **9**, 599 (1994).
[30] L. L. Bonilla and F. J. Higuera, SIAM J. Appl. Math. (to be published).
[31] L. L. Bonilla, Physica D **55**, 182 (1992).
[32] L. L. Bonilla, F. J. Higuera, and S. Venakides, SIAM J. Appl. Math. **54**, 1521 (1994).
[33] I. R. Cantalapiedra, L. L. Bonilla, M. J. Bergmann, and S. W. Teitsworth, Phys. Rev. B **48**, 12 278 (1993).
[34] L. L. Bonilla and S. W. Teitsworth, Physica D **50**, 545 (1991).
[35] S. W. Teitsworth, Appl. Phys. A **48**, 127 (1989).
[36] C. Canali, F. Nava, and L. Reggiani, in *Hot-Electron Transport in Semiconductors*, edited by L. Reggiani, Topics in Applied Physics Vol. 58 (Springer-Verlag, Berlin, 1985).
[37] C. Jacoboni and L. Reggiani, Adv. Phys. **28**, 493 (1979).
[38] S. W. Teitsworth, Ph.D. thesis, Harvard University, 1986.
[39] V. V. Mitin, Appl. Phys. A **39**, 123 (1986).
[40] E. Schöll, Solid State Electron. **31**, 539 (1988).
[41] E. Schöll, Appl. Phys. A **48**, 95 (1989).
[42] T. Kuhn *et al.*, Phys. Rev. B **48**, 1478 (1993).
[43] R. Peyret and T. D. Taylor, in *Computational Methods for Fluid Flow*, edited by H. Cabannes *et al.*, Springer Series in Computational Physics (Springer-Verlag, New York, 1983).
[44] E. G. Gwinn and R. M. Westervelt, Phys. Rev. Lett. **57**, 1060 (1986).
[45] E. G. Gwinn and R. M. Westervelt, Phys. Rev. Lett. **59**, 157 (1987).
[46] Z. Jiang, J. Appl. Phys. **76**, 4159 (1994).
[47] E. Ott, *Chaos in Dynamical Systems* (Cambridge University Press, New York, 1993).
[48] H. G. Schuster, *Deterministic Chaos* (Physik-Verlag, Weinheim, 1984).
[49] P. Bergé, Y. Pomeau, and C. Vidal, *Order within Chaos* (Hermann and John Wiley & Sons, Paris, 1984).
[50] N. Platt, E. A. Spiegel, and C. Tresser, Phys. Rev. Lett. **70**, 279 (1993).
[51] J. F. Heagy, N. Platt, and S. M. Hammel, Phys. Rev. E **49**, 1140 (1994).
[52] F. Xie, G. Hu, and Z. Qu, Phys. Rev. E **52**, 1265 (1995).
[53] P. W. Hammer *et al.*, Phys. Rev. Lett. **73**, 1095 (1994).
[54] Y. H. Yu, K. Kwak, and T. K. Lim, Phys. Lett. **198**, 34 (1995).
[55] A. M. Kahn (private communication).
[56] M. J. Bergmann, S. W. Teitsworth, L. L. Bonilla, and I. R. Cantalapiedra (unpublished).
[57] A. Van Der Ziel, *NOISE: Sources, Characterization, Measurement* (Prentice-Hall, Englewood Cliffs, NJ, 1970).
[58] E. E. Haller, W. L. Hansen, and F. S. Goulding, Adv. Phys. **30**, 93 (1981).
[59] E. E. Haller (private communication).
[60] D. Kincaid and W. Cheney, *Numerical Analysis: Mathematics of Scientific Computing* (Brooks/Cole, Pacific Grove, CA, 1991).